Research Paper
Computational Methods for Differential Equations
http://cmde.tabrizu.ac.ir
Vol. *, No. *, *, pp. 1-21
DOI:10.22034/cmde.2026.68088.3279

Analysis of disease mediated predator-prey system with fractional time derivative under climatic stressors

Sivaranjani Munusamy[1], **Sambath Muniyagounder**[1,*], **and Balachandran Krishnan**[2]

[1]Department of Mathematics, Periyar University, Salem 636011, India.

[2]Department of Mathematics, Bharathiar University, Coimbatore 641046, India.

Abstract

This study presents a novel fractional order dynamical system modeling of disease-mediated predator-prey interactions under climatic stressors. The framework incorporates: (i) temperature dependent growth reduction (ii) wind modulated predation efficiency (iii) disease mediated predator through a time fractional derivative formulation. We thoroughly examine the qualitative properties, in order to establish sufficient conditions for the existence, positivity, and uniqueness of solutions. We also look into the quantitative behavior of the system by analyzing the stability of positive equilibrium points, and derive criteria for both local and global stability. We conduct comprehensive numerical simulations to verify our theoretical conclusions, showing that analytical results remain consistent under different parameteric impacts.

Keywords. Fractional-order predator-prey model, Disease dynamics, Global warming, Wind flow, Stability analysis, Numerical simulations.
2010 Mathematics Subject Classification. 34A08, 34K37, 37N25, 26A33.

1. Introduction

A fractional calculus constitutes a paradigm-shifting framework within mathematical biology, offering a sophisticated mathematical formalism that elegantly bridges the gap between the abstract theoretical constructs and the intricate realities of biological systems. With the rapid evolution of high-performance computational methodologies and the proliferation of cross-disciplinary research synergies, fractional mathematical biology is emerging as a cornerstone for groundbreaking advances in mechanistic disease modeling, spatially heterogeneous ecological interactions, and next-generation biomedical engineering. This developing field promotes a deeper and more comprehensive understanding of the fundamental mathematical concepts underlying biological processes in addition to improving the precision of quantitative predictions. Also, fractional calculus allows a nuanced depiction of how organisms and ecosystems respond over time to temperature fluctuations, altered precipitation, and other climatic pressures [9, 20, 24, 25]. This reveals that biological responses to climate stress are rarely instantaneous or linear, often leading to unexpected shifts in population dynamics, disease spread, and ecosystem stability. These biological responses are effectively regulated by various types of functional mechanisms like Holling type functional responses and others [12, 15, 26, 28]. By embracing the nonlocal and history-dependent nature of these interactions, fractional models offer deeper insight into the resilience and vulnerability of biological systems under the relentless influence of a changing climate's stressors.

Global warming, characterized by rising global temperatures, altered precipitation patterns, and shifting habitat availability, profoundly reshapes predator-prey dynamics across ecosystems. Reduced prey abundance or diminished prey body condition, often a consequence of climate extremes can exacerbate food scarcity for predators, leading to decreased feeding rates and slower predator population growth. In some cases, warming may also reduce ingestion efficiency in predators, increasing their vulnerability to starvation despite higher metabolic rates. Warming can suppress prey metabolism and activity, reducing their capacity to evade predation, while also influencing the production

Received: 11 July 2025; Accepted: 03 June 2026.
∗ Corresponding author. Email: sambathbu2010@gmail.com .

and transmission of sensory cues that mediate predator-prey interactions. Climate-induced temperature shifts alter predator functional responses, affecting predation rates, population dynamics, and species sustainability by modifying predator functional responses [22, 23]. Zimova et al. [33] demonstrated that climate change can restructure predator-prey interactions, with cascading effects on population stability. Similarly, Post et al. [32] documented the ecological consequences of predator behavioral responses to global climate change, emphasizing the role of temperature in shaping trophic dynamics. Laws et al. [15] explains that temperature changes can affect metabolic rates, behavior and distribution of species, leading to altered food web dynamics. Later on Panja [17] investigates that global warming negatively affects the growth rate of prey, which in turn influences predator populations. Sekeri [27] modeled climate variability via fractional derivatives, enabling advanced analytical treatments of ecological stressors in subsequent studies.

Wind flow exhibits varying patterns and speeds, which can influence a species' sensory perception and impact its capacity to recognize predatory signs. The particular predator species involved determines how wind affects predation. Windy conditions may disrupt the movement of certain organisms, reducing predator efficiency by dislodging, slowing, or otherwise hindering them. This leads to decreased predation rates, ultimately benefiting prey populations and wind interference diminishes predator search efficiency, negatively affecting hunting success. Increased wind flow causes predators to search less effectively and handle prey for longer periods of time. On the other side, handling time stays the same when there is no wind. The longer it takes for predators to get prey, the stronger the wind. Extreme wind conditions can make it impossible for predators to find prey at all. In natural environments, wind speed varies throughout time instead of staying steady. As a result, wind needs to be represented as a time-dependent variable. Through the modification of functional responses, Barman et al. [2] investigate how wind can both promote and prevent predation. The impact of periodically fluctuating wind flow on system stability and bifurcation behavior is also examined. Panja [19] discovers that depending on how the wind interacts with the behavior of the prey, it can either stabilize or destabilize the system.

In prey-predator models, disease transmission is typically modeled as a function of direct contact between susceptible and infected individuals, with the transmission rate depending on the frequency and intensity of such interactions. The transmission of the disease to susceptible individuals is facilitated through direct contact with infected individuals, encapsulated by the incidence of transmission term. This process depends on a critical threshold of interaction between susceptible and infected hosts. Notably, the limited mobility of individuals constrains the frequency of such contacts within a given time frame, thereby influencing the overall disease dynamics. The disease transmission only in prey density, only in predator density and in both population density have been studied [4, 7, 10, 11].

Further, Thirthar et al. [30, 31] investigated a model incorporating disease transmission along with global warming, impact of wind flow, effects of predator hunting, prey fear including global warming. Also, they extended the research in fractional-order derivatives which established the axiomatic basis of our framework [8, 13, 28, 29]. From the foregoing investigations, we propose a theoretical framework in which global warming exerts cascading effects on both prey and predator populations in Caputo's sense. Specifically, rising temperatures increase predation rates and predator abundance, thereby intensifying pressure on prey populations. To mitigate this imbalance, disease transmission is introduced as a compensatory mechanism within the predator population. This dynamic reduces predator numbers, alleviating predation pressure on the prey. Furthermore, infected predators impaired in their ability to hunt become dependent on susceptible predators for sustenance.

In this paper, Section 2 deals with the definitions, theorems, and lemmas used throughout the paper and the system is formulated with some assumptions in Section 3. Also, the existence of well-defined unique solution and that solutions remains in a non-negative feasible region are investigated. The general stability analysis of the system is discussed in Section 4. To enhance the above analytical solutions, Section 5 discusses the numerical simulations that impacts the postulated model.

2. Preliminaries

Some basic definitions and properties of fractional calculus are provided in this section [1, 14, 18–21].

Definition 2.1. [1, 14] Let $g : \mathbb{R}^+ \to \mathbb{R}$ be a Lebesgue integrable function. The Riemann-Liouville fractional integral of order $\eta > 0$ is defined as

$$I^{\eta} g(t) = \frac{1}{\Gamma(\eta)} \int_{t_0}^{t} (t-\tau)^{\eta-1} g(\tau) d\tau,$$

and for a sufficiently differentiable function $g(t)$ and $m-1 < \eta < m$, the Caputo fractional order derivative is given by

$$D_t^{\eta} g(t) = \frac{1}{\Gamma(m-\eta)} \int_{t_0}^{t} (t-\tau)^{m-\eta-1} g^{(m)}(\tau) d\tau,$$

where $\Gamma(\eta)$ is the Euler's Gamma function.

Lemma 2.2. *[1, 3] Let $0 < \eta \leq 1$ and $\rho < 0$. Then, $E_{\eta,\eta}(\rho t^{\eta})$ and $E_{\eta,\eta+1}(\rho t^{\eta})$ tend monotonically to zero as $t \to \infty$.*

Lemma 2.3. *[1, 3]Let $0 < \eta < 1$ and $|\arg(\rho)| > \pi\eta/2$. Then, one has $t^{\eta} E_{\eta,\eta+1}(\gamma t^{\eta}) = \frac{1}{\rho} - \frac{1}{\Gamma(1-\eta)\rho^2 t^{\eta}} + O\left(\frac{1}{\rho^2 t^{\eta}}\right)$, as $t \to \infty$.*

Here $E_{\alpha,\alpha}(\cdot)$ is a two parameter family of Mittag-Leffler function [14, 21].

Theorem 2.4. *[18, 20] Consider the fractional-order system*

$$\begin{cases} D_t^{\eta} \boldsymbol{P_i}(t) = g(\boldsymbol{P_i}), \\ \boldsymbol{P_i}(t_0) = \boldsymbol{P_{i_0}}, \qquad with \quad \eta \in (0,1) and \quad \boldsymbol{P_i} \in R_+^3, i = (x,y,z). \end{cases}$$

This equilibrium point $\boldsymbol{P_i^*}$ is l.a.s (locally asymptotically stable) if all the eigenvalues ψ_j of the Jacobian matrix $J = \frac{\partial g(\boldsymbol{P_i^*})}{\partial \boldsymbol{P_i}}$ satisfy $|arg(\psi_j)| > \frac{\eta\pi}{2}$.

Theorem 2.5. *[19] Assume the function $g(t) \in \mathbb{R}^+$ that implies continuity and differentiability. Then, for any time $t > t_0$,*

$$\mathcal{D}_t^{\eta} \left[g(t) - g^* - g^* \ln \frac{g(t)}{g^*} \right] \leq \left(1 - \frac{g^*}{g(t)}\right) \mathcal{D}_t^{\eta} g(t), g^* \in \mathbb{R}^+, \forall \eta \in (0,1).$$

3. Formulation of the system

The fractional-order system is postulated under the following assumptions:

(1) Let P_x, P_y and P_z are denoted as the prey, the meso predator, the apex predator respectively. The prey density P_x follows logistic growth with an intrinsic rate $r > 0$ and carrying capacity $k > 0$. The impact of global warming on prey population dynamics is modeled by the term:

$$\psi(P_x) = \frac{1}{1 + g_1 P_x},$$

where $g_1 > 0$ represents the global warming intensity coefficient on prey. The global warming effect exhibits the following limiting behaviors:

- As $g_1 \to 0^+$, the global warming effect becomes negligible:

$$\lim_{g_1 \to 0^+} \psi(P_x) = 1.$$

- As $g_1 \to \infty$, the global warming effect dominates:

$$\lim_{g_1 \to \infty} \psi(P_x) = 0.$$

(2) The mesopredator P_y exhibits a functional response, which is nonlinear $\frac{(1+g_2 P_y)(1+w_f) P_x P_y}{1+h(1+g_2 P_y)(1+w_f) P_x}$. Here, we assume $\frac{1}{1+g_2 P_y}$, $g_2 > 0$ is the global warming intensity coefficient on predators that quantifies the temperature-dependent modulation of predator hunting efficiency. We examine the limiting behavior of the system under two extreme climatic scenarios:

- As $g_2 \to 0^+$, the functional response reduces to classical Beddington-DeAngelis form:

$$\mathcal{F}(P_x, P_y) \to \frac{(1+w_f)P_xP_y}{1+h(1+w_f)P_x},$$

  where predation remains strictly prey-limited, it reduces to standard predator-prey dynamics with baseline hunting efficiency $(1+w_f)$, unaffected by warming-induced changes in predation.
- As $g_2 \to \infty$, the predation dynamics exhibit saturation behavior:

$$\mathcal{F}(P_x, P_y) \to \frac{P_y}{h},$$

  where the prey population density loses its dependence on predator abundance, and predator population growth approaches a maximum rate constrained solely by the handling time h.

(3) $\xi(w_f) = 1 + w_f$ is the wind flow dependent on the handling time (h) of the prey density with the following hypothetical assumptions:
- $\xi(0) = 1$, no wind implies no change in handling time.
- $\xi'(w_f) > 0$ for all $w_f > 0$, handling time increases with wind speed.

(4) The apex predator P_z exhibits functional response $\frac{\delta P_y P_z}{P_y+P_z}$ that represents the transmission of disease to the meso predator. The disease transmission rate is denoted by δ.

(5) We also denote that m_1 and m_2 are the fatality rate of the meso and the apex predators respectively.

By the above-mentioned assumptions, the system of Caputo fractional differential equations that modeled the temporal evolution of the prey-predator system is given by:

$$\begin{aligned}
D_t^\eta P_x &= \frac{rP_x}{1+g_1P_x}\left(1-\frac{P_x}{k}\right) - \frac{(1+g_2P_y)\,(1+w_f)\,P_xP_y}{1+h\,(1+g_2P_y)\,(1+w_f)\,P_x},\\
D_t^\eta P_y &= \frac{(1+g_2P_y)\,(1+w_f)\,P_xP_y}{1+h\,(1+g_2P_y)\,(1+w_f)\,P_x} - \frac{\delta P_yP_z}{P_y+P_z} - m_1P_y,\\
D_t^\eta P_z &= \frac{\delta P_yP_z}{P_y+P_z} - m_2P_z,
\end{aligned} \tag{3.1}$$

with the prerequisites of the system (3.1) of order $\eta \in (0,1)$:

$$P_x(t_0) = P_{x_0} \geq 0, \quad P_y(t_0) = P_{y_0} \geq 0, \quad P_z(t_0) = P_{z_0} \geq 0. \tag{3.2}$$

Define $\aleph = \{(P_x, P_y, P_z) \in \mathbb{R}^3_+ : \max(|P_x|, |P_y|, |P_z|) \leq N\}$ for some $N > 0$.

3.1. **Existence of a unique well-defined solution.**

Theorem 3.1. *Given an arbitrary non-negative prerequisites of the sytem (3.1), determines a unique solution* $Y(t) \in \aleph$, $\forall t \geq t_0$.

Proof. Given that an appropriate prerequisites in the region $\aleph \times (t_0, T]$, $T < \infty$. Let us consider the solutions of the system be $Y = (P_x, P_y, P_z)$ and $\hat{Y} = (\hat{P_x}, \hat{P_y}, \hat{P_z})$. Let $P(Y) = (P_1(Y), P_2(Y), P_3(Y))$ and

$$\begin{aligned}
P_1(Y) &= \frac{rP_x}{1+g_1P_x}\left(1-\frac{P_x}{k}\right) - \frac{(1+g_2P_y)\,(1+w_f)\,P_xP_y}{1+h\,(1+g_2P_y)\,(1+w_f)\,P_x},\\
P_2(Y) &= \frac{(1+g_2P_y)(1+w_f)P_x^2P_y}{1+h(1+g_2P_y)(1+w_f)P_x^2} - \frac{\delta P_y^2P_z^2}{P_y^2+P_z^2} - m_1P_y,\\
P_3(Y) &= \frac{\delta P_yP_z}{P_y+P_z} - m_2P_z.
\end{aligned}$$

For any $Y, \hat{Y} \in \aleph$, we have

$$\|P(Y) - P(\hat{Y})\| = |P_1(Y) - P_1(\hat{Y})| + |P_2(Y) - P_2(\hat{Y})| + |P_3(Y) - P_3(\hat{Y})|$$

$$
\begin{aligned}
&= \left| \frac{rP_x}{1+g_1P_x}\left(1-\frac{P_x}{k}\right) - \frac{(1+g_2P_y)(1+w_f)P_xP_y}{1+h(1+g_2P_y)(1+w_f)P_x} - \frac{r\hat{P}_x}{1+g_1\hat{P}_x}\left(1-\frac{\hat{P}_x}{k}\right) \right. \\
&+ \left. \frac{(1+g_2\hat{P}_y)(1+w_f)\hat{P}_x\hat{P}_y}{1+h(1+g_2\hat{P}_y)(1+w_f)\hat{P}_x} \right| + \left| \frac{(1+g_2P_y)(1+w_f)P_xP_y}{1+h(1+g_2P_y)(1+w_f)P_x} - \frac{\delta P_yP_z}{P_y+P_z} \right. \\
&- m_1P_y - \left. \frac{(1+g_2\hat{P}_y)(1+w_f)\hat{P}_x\hat{P}_y}{1+h(1+g_2\hat{P}_y)(1+w_f)\hat{P}_x} + \frac{\delta\hat{P}_y\hat{P}_z}{\hat{P}_y+\hat{P}_z} + m_1\hat{P}_y \right| + \left| \frac{\delta P_yP_z}{P_y+P_z} - m_2P_z - \frac{\delta\hat{P}_y\hat{P}_z}{\hat{P}_y+\hat{P}_z} + m_2\hat{P}_z \right| \\
&\leq \left| r.\frac{P_x-\hat{P}_x}{(1+g_1P_x)(1+g_1\hat{P}_x)} - \left(\frac{r}{k}.\frac{{P_x}^2}{(1+g_1P_x)} - \frac{{\hat{P}_x}^2}{k(1+g_1\hat{P}_x)} \right) - \left(\frac{(1+g_2P_y)(1+w_f)P_xP_y}{1+h(1+g_2P_y)(1+w_f)P_x} \right. \right. \\
&- \left. \left. \frac{(1+g_2\hat{P}_y)(1+w_f)\hat{P}_x\hat{P}_y}{1+h(1+g_2\hat{P}_y)(1+w_f)\hat{P}_x} \right) \right| + \left| -\delta\left(\frac{P_yP_z}{P_y+P_z} - \frac{\hat{P}_y\hat{P}_z}{\hat{P}_y+\hat{P}_z} \right) - (m_1P_y - m_1\hat{P}_y) \right. \\
&+ \left. \left(\frac{(1+g_2P_y)(1+w_f)P_xP_y}{1+h(1+g_2P_y)(1+w_f)P_x} - \frac{(1+g_2\hat{P}_y)(1+w_f)\hat{P}_x\hat{P}_y}{1+h(1+g_2\hat{P}_y)(1+w_f)\hat{P}_x} \right) \right| \\
&+ \left| \delta\left(\frac{P_yP_z}{P_y+P_z} - \frac{\hat{P}_y\hat{P}_z}{\hat{P}_y+\hat{P}_z} \right) - (m_2P_z - m_2\hat{P}_z) \right| \\
&\leq \left| r.\frac{P_x-\hat{P}_x}{(1+g_1P_x)(1+g_1\hat{P}_x)} - \left(\frac{r}{k}.\frac{({P_x}^2-{\hat{P}_x}^2)+g_1(\hat{P}_x{P_x}^2-P_x{\hat{P}_x}^2)}{(1+g_1P_x)(1+g_1\hat{P}_x)} \right) \right. \\
&- \frac{1}{\big(1+h(1+g_2P_y)(1+w_f)P_x\big)\big(1+h(1+g_2\hat{P}_y)(1+w_f)\hat{P}_x\big)} \Big[(1+w_f)\hat{P}_x(1+g_2\hat{P}_x)(P_x-\hat{P}_x) \\
&+ \left. (1+w_f)\left(P_x(1+h(1+g_2(P_y+\hat{P}_y)) + h(1+g_2P_y)(1+g_2\hat{P}_y)(1+w_f)P_x\hat{P}_x \right)(P_y-\hat{P}_y) \Big] \right| \\
&+ \left| \frac{1}{\big(1+h(1+g_2P_y)(1+w_f)P_x\big)\big(1+h(1+g_2\hat{P}_y)(1+w_f)\hat{P}_x\big)} \Big[(1+w_f)\hat{P}_x(1+g_2\hat{P}_x)(P_x-\hat{P}_x) \right. \\
&+ \left. (1+w_f)\left(P_x(1+h(1+g_2(P_y+\hat{P}_y)) + h(1+g_2P_y)(1+g_2\hat{P}_y)(1+w_f)P_x\hat{P}_x \right)(P_y-\hat{P}_y) \Big] \right. \\
&- \delta\Big(P_y\hat{P}_y(P_z-\hat{P}_z) - P_z\hat{P}_z(P_y-\hat{P}_y) \Big) - m_1(P_y-\hat{P}_y) \Big| + \Big| \delta\Big(P_y\hat{P}_y(P_z-\hat{P}_z) \\
&- P_z\hat{P}_z(P_y-\hat{P}_y) \Big) - m_2(P_z-\hat{P}_z) \Big| \\
&\leq (r(1+2N+g_1N^2) + (1+w_f)(1+g_2N)N)|P_x-\hat{P}_x| \\
&+ (1+w_f)((1+2g_2N)N + h(1+g_2N)^2N^2)|P_y-\hat{P}_y| \\
&+ (1+w_f)(1+g_2N)N)|P_x-\hat{P}_x| \\
&+ ((1+2g_2N)N + h(1+g_2N)^2N^2 + \delta N^2 + 2\delta N^2 + m_1)|P_y-\hat{P}_y| \\
&+ \delta N^2|P_z-\hat{P}_z| + (\delta N^2+m_2)|P_z-\hat{P}_z| + \delta N^2|P_y-\hat{P}_y| \\
&\leq (r(1+2N+g_1N^2) + 2N(1+w_f)(1+g_2N))|P_x-\hat{P}_x| \\
&+ 2((1+2g_2N)N + h(1+g_2N)^2N^2 + m_1)|P_y-\hat{P}_y| + (2\delta N^2+m_2)|P_z-\hat{P}_z| \\
&\leq M_1|P_x-\hat{P}_x| + M_2|P_y-\hat{P}_y| + M_3|P_z-\hat{P}_z|,
\end{aligned}
$$

where, $M_1 = r(1+2N+g_1N^2) + 2N(1+w_f)(1+g_2N)$, $M_2 = 2((1+2g_2N)N + h(1+g_2N)^2N^2 + m_1)$, and $M_3 = 2\delta N^2 + m_2$. By assuming $M > 0$, $M = \max\{M_1, M_2, M_3\}$, resulting in $\|P(Y) - P(\hat{Y})\| \leq M\|Y - \hat{Y}\|$. Thus, the sytem (3.1) determines a unique solution $Y(t)$ and $P(Y)$ fulfills the Lipschitz condition. □

3.2. **Existence of non-negative and confined solutions.**

Theorem 3.2. *A solution of the system (3.1) that starts from* $(P_{x_0}, P_{y_0}, P_{z_0}) \in \mathbb{R}^3_+$ *lies non negative within the feasible region* Φ.

Proof. The following function is considered as

$$P_u(t) = P_x(t) + P_y(t) + P_z(t).$$

Taking Caputo's derivative on both sides, resulting in

$$\begin{aligned} D^\eta_t P_u(t) &= D^\eta_t P_x(t) + D^\eta_t P_y(t) + D^\eta_t P_z(t) \\ &= \frac{rP_x}{1+g_1P_x}\left(1-\frac{P_x}{k}\right) - \frac{(1+g_2P_y)(1+w_f)P_xP_y}{1+h(1+g_2P_y)(1+w_f)P_x} \\ &+ \frac{(1+g_2P_y)(1+w_f)P_xP_y}{1+h(1+g_2P_y)(1+w_f)P_x} - \frac{\delta P_yP_z}{P_y+P_z} - m_1P_y + \frac{\delta P_yP_z}{P_y+P_z} - m_2P_z \\ &= \frac{rP_x}{1+g_1P_x}\left(1-\frac{P_x}{k}\right) - m_1P_y - m_2P_z. \end{aligned}$$

For each $\rho > 0$, implies that

$$\begin{aligned} D^\eta_t P_u(t) + \rho P_u(t) =& \frac{rP_x}{1+g_1P_x}\left(1-\frac{P_x}{k}\right) - m_1P_y - m_2P_z + \rho(P_x+P_y+P_z) \\ \le& \frac{rP_x}{1+g_1P_x}\left(1-\frac{P_x}{k}\right) + \rho P_x - (m_1-\rho)P_y - (m_2-\rho)P_z \\ \le& \frac{rP_x}{1+g_1P_x}\left(1-\frac{P_x}{k}+\rho\right), \end{aligned}$$

where $\rho < \min\{r, m_1, m_2\}$. Considering that $h(P_x) = \frac{rP_x}{1+g_1P_x}\left(1-\frac{P_x}{k}+\rho\right)$, then the maximum of $h(P_x)$ at $P_x = \frac{k(1+\rho)}{2}$ is $\max h(P_x) = \frac{rk(1+\rho)^2}{4}$. Thus, from the previous equation, implies that

$$D^\eta_t P_u(t) + \rho P_u(t) \le \frac{rk(1+\rho)^2}{4}.$$

Let $P_u(0) = P_{u_0}$ be the initial condition, by comparison principle [19, 21]

$$\begin{aligned} P_u(t) \le& P_{u_0}E_\eta(-\rho t^\eta) + \frac{rk(1+\rho)^2}{4}\int_0^s (t-s)^{\eta-1}E_{\eta,\eta}(-\rho(t-s)^\eta)ds \\ =& P_{u_0}E_\eta(-\rho t^\eta) + \frac{rk(1+\rho)^2}{4}\int_0^s (t-s)^{\eta-1}\sum_{i=0}^{\infty}\frac{(-\rho)^i(t-s)^{\eta i})}{\Gamma(i\eta+\eta)}ds \\ =& P_{u_0}E_\eta(-\rho t^\eta) + \frac{rk(1+\rho)^2}{4}\sum_{i=0}^{\infty}\frac{(-\rho)^i}{\Gamma(i\eta+\eta)}\int_0^s (t-s)^{\eta(i+1)-1}ds \\ =& P_{u_0}E_\eta(-\rho t^\eta) + \frac{rk(1+\rho)^2}{4}\sum_{i=0}^{\infty}\frac{(-\rho)^i t^{\eta i}}{\Gamma(i\eta+\eta+1)} \\ =& P_{u_0}E_\eta(-\rho t^\eta) + \frac{rk(1+\rho)^2}{4}t^\eta E_{\eta,\eta+1}(-\rho t^\eta). \end{aligned}$$

Applying Lemma (2.2),

$$E_{\eta,\eta}(-\rho t^{\eta}) = -\sum_{i=1}^{2} \frac{1}{\Gamma(\eta-\eta i)} \frac{1}{(-\rho)^i t^{\eta i}} + O\left(\frac{1}{(-\rho)^3 t^{2\eta}}\right)$$
$$= -\frac{1}{\Gamma(-\rho)} \frac{1}{(-\rho)^2 t^{2\eta}} \to 0 \quad \text{as } t \to \infty.$$

Then, from applying Lemma (2.3),

$$t^{\eta} E_{\eta,\eta+1}(-\rho t^{\eta}) = \frac{1}{\rho} - \frac{1}{\Gamma(1-\eta(-\rho)^2 t^{\eta})} + O\left(\frac{1}{(-\rho)^3 t^{2\eta}}\right)$$
$$= \frac{1}{\rho} \quad \text{as } t \to \infty.$$

Hence, it is obtained that,

$$P_u(t) \leq \frac{rk(1+\rho)^2}{4}.$$

Consequently, the solutions of the system (3.1) in $\mathbb{R}^3_+$ stays constrained in the feasible region that is non negatively variant

$$\Phi = \{(P_x, P_y, P_z) \in \mathbb{R}^3_+ : P_u(t) = \frac{rk(1+\rho)^2}{4\rho} + \epsilon, \epsilon > 0\}.$$

□

4. General stability analysis of the system

In this section, we examine the positive equilibrium points, the local and global stability behavior of the equilibrium points of the given fractional-order system.

4.1. **Local stability of the system.** All the feasible equilibrium points of the given system (3.1) is obtained by the roots of the following equations:

$$\begin{aligned} &\frac{rP_x}{1+g_1P_x}\left(1-\frac{P_x}{k}\right) - \frac{(1+g_2P_y)(1+w_f)P_xP_y}{1+h(1+g_2P_y)(1+w_f)P_x} = 0, \\ &\frac{(1+g_2P_y)(1+w_f)P_xP_y}{1+h(1+g_2P_y)(1+w_f)P_x} - \frac{\delta P_yP_z}{P_y+P_z} - m_1P_y = 0, \\ &\frac{\delta P_yP_z}{P_y+P_z} - m_2P_z = 0. \end{aligned} \tag{4.1}$$

The biologically viable equilibrium points of the system (3.1) are:

(1) The trivial equilibrium point $\Omega(0,0,0) = (0,0,0)$ exists, where the population densities approaches to extinction state.
(2) The only prey population equilibrium point $\Omega(P_x,0,0) = (k,0,0)$ exists, where the meso and apex predators vanishes.
(3) The no apex predator equilibrium point $\Omega(P_x,P_y,0) = (P_{x_1},P_{y_1},0)$, exists if $0 < m_1h < 1$ where $P_{x_1} = \frac{m_1}{(1+g_2P_{y_1})(1+w_f)(1-m_1h)}$ and P_{y_1} can be obtained by the cubic equation as follows:

$aP_{y_1}^3 + bP_{y_1}^2 + cP_{y_1} + d = 0,$
where,

$$a = g_2^2(1+w_f)(1-m_1h), \quad b = 2g_2(1+w_f)(1-m_1h) + g_1g_2m_1,$$
$$c = (1+w_f)(1-m_1h) + g_1m_1 - \frac{rg_2(1+w_f)(1-m_1h)}{1-m_1h}, \quad d = -\frac{r((1+w_f)(1-m_1h)k - m_1)}{k(1-m_1h)^2(1+w_f)}.$$

where we can see that $a, b > 0$ and the cubic equation has a positive root if $c < 0$, i.e, $r > \frac{(1-m_1h)(1+w_f)+g_1m_1}{g_2(1+w_f)}$ and if $d < 0$, i.e, $(1+w_f)(1-m_1h)k > m_1$. Hence, applying the Descartes' Rule of Signs, the no apex predator equilibrium point $\Omega(P_x, P_y, 0)$ exists under the following conditions $r > \frac{(1-m_1h)(1+w_f)+g_1m_1}{g_2(1+w_f)}$ and $(1+w_f)(1-m_1h)k > m_1$.

(4) The coexistence equilibrium point $\Omega(P_x, P_y, P_z) = (P_x^*, P_y^*, P_z^*)$ exists if $h(\delta - m_2 + m_1) < 1$ where $P_x^* = \frac{\delta - m_2 + m_1}{(1+g_2P_y^*)(1+w_f)(1-h(\delta-m_2+m_1))}$, and P_y^* is obtained from the quadratic equation:

$$a_1P_y^{*2} + b_1P_y^* + c_1 = 0,$$

where,

$$a_1 = g_2\left((1+w_f)(1-h(\delta-m_2+m_1)) + g_1(\delta-m_2+m_1)\right),$$
$$b_1 = (1+w_f)(1-h(\delta-m_2+m_1)) + g_1(\delta-m_2+m_1) - rg_2,$$
$$c_1 = \frac{r(\delta-m_2+m_1)}{k(1+w_f)(1-h(\delta-m_2+m_1))} - r,$$

we know that $a_1 > 0$, applying Descarte's Rule of Signs, the positive root exists if $b_1 < 0$ and $c_1 < 0$, i.e,

$$P_y^* = \frac{-b_1 - \sqrt{b_1^2 - 4a_1c_1}}{2a_1}$$

and if $\delta > m_2$ where $P_z^* = \frac{(\delta-m_2)}{m_2}P_y^*$.

The Jacobian matrix $J(\Omega(P_x, P_y, P_z))$ of the fractional-order system (3.1) for the equilibrium point $\Omega(P_x, P_y, P_z) = (P_x, P_y, P_z)$

$$J(\Omega(P_x, P_y, P_z)) = \begin{bmatrix} p_{11} & p_{12} & p_{13} \\ p_{21} & p_{22} & p_{23} \\ p_{31} & p_{32} & p_{33} \end{bmatrix}, \tag{4.2}$$

where,

$$p_{11} = \frac{r}{(1+g_1P_x)^2}\left(1 - \frac{P_x(2+g_1P_x)}{k}\right) - \frac{(1+g_2P_y^*)(1+w_f)P_y}{\left[1+h(1+g_2P_y)(1+w_f)P_x\right]^2},$$
$$p_{12} = -\frac{(1+w_f)\left[1+2g_2P_y+h(1+g_2P_y)^2(1+w_f)P_x\right]}{\left[1+h(1+g_2P_y)(1+w_f)P_x\right]^2}, \quad p_{13} = 0,$$
$$p_{21} = \frac{(1+g_2P_y)(1+w_f)P_y}{\left[1+h(1+g_2P_y)(1+w_f)P_x\right]^2},$$
$$p_{22} = \frac{(1+w_f)\left[1+2g_2P_y+h(1+g_2P_y)^2(1+w_f)P_x\right]}{\left[1+h(1+g_2P_y)(1+w_f)P_x\right]^2} - \frac{\delta P_z^2}{(P_y+P_z)^2} - m_1,$$
$$p_{23} = -\frac{\delta P_y^2}{(P_y+P_z)^2}, \quad p_{31} = 0, \quad p_{32} = \frac{\delta P_z^2}{(P_y+P_z)^2}, \quad p_{33} = \frac{\delta P_y^2}{(P_y+P_z)^2} - m_2 = 0.$$

Theorem 4.1. *The unstable trivial equilibrium point $\Omega(0,0,0) = (0,0,0)$ of a system (3.1) exists.*

Proof. The Jacobian matrix $J(\Omega(0,0,0))$ at the equilibrium point $\Omega(0,0,0) = (0,0,0)$ is

$$J(\Omega(0,0,0)) = \begin{bmatrix} r & 0 & 0 \\ 0 & -m_1 & 0 \\ 0 & 0 & -m_2 \end{bmatrix}.$$

The characteristic equation of the Jacobian matrix $J(\Omega(0,0,0))$ is

$$(r-\phi_1)(-m_1-\phi_2)(-m_2-\phi_3) = 0. \tag{4.3}$$

Hence, $\phi_1 = r(> 0)$, $\phi_2 = -m_1(< 0)$ and $\phi_3 = -m_2(< 0)$ are the eigen values of $\Omega(0,0,0)$. Then, $|arg\ \phi_1| = 0 < \eta\frac{\pi}{2}, |arg\ \phi_2| = \pi > \eta\frac{\pi}{2}, |arg\ \phi_3| = \pi > \eta\frac{\pi}{2}$. By Theorem 2.4, the unstable trivial equilibrium exists. □

Theorem 4.2. *The only prey equilibrium point $\Omega(P_x, 0, 0) = (k, 0, 0)$ is locally asymptotically stable if $\frac{(1+w_f)}{1+h(1+w_f)k} < m_1$.*

Proof. The Jacobian matrix $J(\Omega(P_x, 0, 0))$ at the equilibrium point $\Omega(P_x, 0, 0) = (k, 0, 0)$ is

$$J(\Omega(P_x,0,0)) = \begin{bmatrix} -\frac{r}{1+g_1k} & -\frac{1+w_f}{1+h(1+w_f)k} & 0 \\ 0 & \frac{1+w_f}{1+h(1+w_f)k} - m_1 & 0 \\ 0 & 0 & -m_2 \end{bmatrix}. \tag{4.4}$$

The Jacobian matrix $J\Omega(P_x, 0, 0)$ consists of the characteristic equation

$$\left(-\frac{r}{1+g_1k} - \phi_1\right)\left(\frac{1+w_f}{1+h(1+w_f)k} - m_1 - \phi_2\right)(-m_2 - \phi_3) = 0. \tag{4.5}$$

Hence, $\phi_1 = -\frac{r}{1+g_1k}(< 0)$, $\phi_2 = \frac{1+w_f}{1+h(1+w_f)k} - m_1(< 0)$ and $\phi_3 = -m_2(< 0)$ are the eigenvalues of $\Omega(P_x, 0, 0)$. Then, $|arg\phi_1| = \pi > \eta\frac{\pi}{2}, |arg\phi_2| = \pi > \eta\frac{\pi}{2}, |arg\phi_3| = \pi > \eta\frac{\pi}{2}$. By Theorem 2.4, the only prey equilibrium $\Omega(P_x, 0, 0) = (k, 0, 0)$ is locally asymptotically stable if $\frac{1+w_f}{1+h(1+w_f)k} < m_1$. □

Theorem 4.3. *The no apex predator equilibrium $\Omega(P_x, P_y, 0) = (P_{x_1}, P_{y_1}, 0)$ is locally asymptotically stable if $\delta < m_2$, $a_2 < 0$ and $b_2 > 0$.*

Proof. The Jacobian matrix $J(\Omega(P_x, P_y, 0))$ at the equilibrium point $\Omega(P_x, P_y, 0) = (P_{x_1}, P_{y_1}, 0)$ is

$$J(\Omega(P_x,P_y,0)) = \begin{bmatrix} p_{11} & p_{12} & 0 \\ p_{21} & p_{22} & \delta \\ 0 & 0 & \delta - m_2 \end{bmatrix},$$

where

$$\begin{aligned}
p_{11} &= \frac{r}{(1+g_1P_{x_1})^2}\left(1 - \frac{P_{x_1}(2+g_1P_{x_1})}{k}\right) - \frac{(1+g_2P_{y_1})(1+w_f)P_{y_1}}{[1+h(1+g_2P_{y_1})(1+w_f)P_{x_1}]^2}, \\
p_{12} &= -\frac{(1+w_f)\left[1+2g_2P_{y_1}+h(1+g_2P_{y_1})^2(1+w_f)P_{x_1}\right]}{[1+h(1+g_2P_{y_1})(1+w_f)P_{x_1}]^2}, \\
p_{21} &= \frac{(1+g_2P_{y_1})(1+w_f)P_{y_1}}{[1+h(1+g_2P_{y_1})(1+w_f)P_{x_1}]^2}, \\
p_{22} &= \frac{(1+w_f)\left[1+2g_2P_{y_1}+h(1+g_2P_{y_1})^2(1+w_f)P_{x_1}\right]}{[1+h(1+g_2P_{y_1})(1+w_f)P_{x_1}]^2} - m_1.
\end{aligned}$$

The characteristic equation exhibits from the Jacobian matrix $J(\Omega(P_x, P_y, 0))$ is given as

$$(\delta - m_2 - \phi_1)(\phi^2 - a_2\phi + b_2) = 0. \tag{4.6}$$

It is clear that $\phi_1 = \delta - m_2(< 0)$ if $\delta < m_2$, thus we get $|arg\phi_1| = \pi > \eta\frac{\pi}{2}$. Then, the other roots $\phi_{2,3}$ is given by the equation $(\phi^2 - a_2\phi + b_2) = 0$, then

$$\phi_{2,3} = \frac{a_2 \pm \sqrt{a_2^2 - 4b_2}}{2},$$

where $a_2 = p_{11} + p_{22} < 0$ and $b_2 = p_{11}p_{22} - p_{12}p_{21} > 0$. Hence, under the following conditions if $\delta < m_2$, $a_2 < 0$ and $b_2 > 0$, the no apex predator equilibrium $\Omega(P_x, P_y, 0) = (P_{x_1}, P_{y_1}, 0)$ is locally asymptotically stable.

□

Theorem 4.4. *The coexistence equilibrium point $\Omega(P_x, P_y, P_z) = (P_x^*, P_y^*, P_z^*)$ is locally asymptotically stable.*

Proof. The equilibrium point $\Omega(P_x, P_y, P_z) = (P_x^*, P_y^*, P_z^*)$ is consists of the Jacobian matrix $J(\Omega(P_x, P_y, P_z))$:

$$J(\Omega(P_x, P_y, P_z)) = [p_{ij}]_{3\times 3}, \tag{4.7}$$

consists of entries as same as in the matrix (4.2). The corresponding characteristic equation Ψ of the Jacobian matrix $J(\Omega(P_x, P_y, P_z))$ is

$$\phi_1^3 + V_1\phi_2^2 + V_2\phi_3 + V_3 = 0, \tag{4.8}$$

where

$$\begin{aligned} V_1 &= -(p_{11} + p_{22} + p_{33}),\\ V_2 &= p_{22}p_{33} + p_{11}(p_{22} + p_{33}) - (p_{12}p_{21} + p_{23}p_{32}),\\ V_3 &= p_{32}(p_{11}p_{23} - p_{13}b_{21}) + p_{33}(p_{12}p_{21} - p_{11}p_{22}). \end{aligned}$$

Consequently, the coexistence equilibrium point $\Omega(P_x, P_y, P_z) = (P_x^*, P_y^*, P_z^*)$ is locally aysmptotically stable if at least one of the following conditions is true:

- If $\mathcal{D}(\Psi) > 0, V_1 > 0, V_3 > 0$ and $V_1V_2 - V_3 > 0$, for $\eta \in (0, 1)$.
- If $\mathcal{D}(\Psi) < 0, V_1 \geq 0, V_2 \geq 0$, and $V_3 > 0$, $0 < \eta < 2/3$.
- If $\mathcal{D}(\Psi) < 0, V_1 > 0, V_2 > 0$, and $V_1V_2 = V_3$, for $0 < \eta < 1$.

□

4.2. **Existence of a Hopf bifurcation.**

Theorem 4.5. *Let Ω^* is an equilibrium point of the system (3.1), reaches a Hopf bifurcation at the equilibrium point Ω^* with respect to the parameter $\nu(\eta, g_1, g_2, w_f, \delta)$ at $\nu = \nu^*(\eta^*, g_1^*, g_2^*, w_f^*, \delta^*)$, if it satisfies the following:*

1. *The Jacobian matrix $J(\Omega(P_x, P_y, P_z))$ of the system (3.1) at the equilibrium point Ω^* has a pair of eigen values which is a complex conjugate $\phi_{1,2} = \gamma \pm i\omega$, at $\nu(\eta, g_1, g_2, w_f, \delta) = \nu^*(\eta^*, g_1^*, g_2^*, w_f^*, \delta^*)$ it becomes purely imaginary.*
2. $m(\nu^*(\eta^*, g_1^*, g_2^*, w_f^*, \delta^*)) = \nu^*(\eta^*, g_1^*, g_2^*, w_f^*, \delta^*)\frac{\pi}{2} - \min_{1\leq i\leq 2} |arg\phi_i| = 0.$
3. $\frac{dm(\nu(\eta,g_1,g_2,w_f,\delta))}{d\nu}|_{\nu(\eta,g_1,g_2,w_f,\delta)-\nu^*(\eta^*,g_1^*,g_2^*,w_f^*,\delta^*)} \neq 0.$

Proof. Given the Jacobian matrix of system (3.1) at Ω^* yields the characteristic equation $\phi^3 + V_1(\nu)\phi^2 + V_2(\nu)\phi + V_3(\nu) = 0$, where V_1, V_2, V_3 are smooth functions on ν. Let the eigenvalues be $\phi_1(\nu) = \gamma(\nu) + i\omega(\nu)$, $\phi_2(\nu) = \gamma(\nu) - i\omega(\nu)$, $\phi_3(\nu) \in \mathbb{R}^-$. Define the bifurcation function $m(\nu) = \frac{\eta\pi}{2} - \min_{1\leq i\leq 3} |\arg(\phi_i(\nu))|$. Since ϕ_3 is real and negative, $|\arg(\phi_3)| = \pi > \eta\pi/2$. Thus $m(\nu) = \frac{\eta\pi}{2} - |\arg(\phi_1(\nu))|$. Condition (2) of the theorem, $m(\nu^*) = 0$, is equivalent to

$$|\arg(\phi_1(\nu^*))| = \frac{\eta\pi}{2} \iff \frac{\omega(\nu^*)}{\gamma(\nu^*)} = \tan\left(\frac{\eta\pi}{2}\right). \tag{4.9}$$

For $\eta \in (0, 1)$, this implies $\gamma(\nu^*) > 0$. Now, it is needed to show that as ν crosses ν^*, the function $m(\nu)$ changes sign with nonzero slope. Let $\theta(\nu) = |\arg(\phi_1(\nu))| = \tan^{-1}(\omega(\nu)/\gamma(\nu))$. Then $\frac{d\theta}{d\nu} = \frac{1}{1+(\omega/\gamma)^2} \cdot \frac{\gamma\omega' - \omega\gamma'}{\gamma^2}$, where $\gamma' = d\gamma/d\nu$, $\omega' = d\omega/d\nu$. Using (4.9) at $\nu = \nu^*$, we have $\omega/\gamma = \tan(\eta\pi/2)$, so $1 + (\omega/\gamma)^2 = 1/\cos^2(\eta\pi/2)$. Therefore

$$\left.\frac{dm}{d\nu}\right|_{\nu^*} = -\left.\frac{d\theta}{d\nu}\right|_{\nu^*} = -\cos^2\left(\frac{\eta\pi}{2}\right) \cdot \left.\frac{\gamma\omega' - \omega\gamma'}{\gamma^2}\right|_{\nu^*}. \tag{4.10}$$

Thus, transversality ($\frac{dm}{d\nu} \neq 0$ at ν^*) is equivalent to

$$\gamma(\nu^*)\omega'(\nu^*) - \omega(\nu^*)\gamma'(\nu^*) \neq 0. \tag{4.11}$$

Now, substitute $\phi = \gamma + i\omega$ into (4.8) and separate real and imaginary parts:

$$\begin{cases} A(\nu) = \gamma^3 - 3\gamma\omega^2 + V_1(\gamma^2 - \omega^2) + V_2\gamma + V_3 = 0,\\ B(\nu) = 3\gamma^2\omega - \omega^3 + 2V_1\gamma\omega + V_2\omega = 0. \end{cases} \tag{4.12}$$

Differentiate A and B with respect to ν at ν^*: $\frac{dA}{d\nu} = \Phi_1\gamma' - \Phi_2\omega' + \Phi_3 = 0$, $\frac{dB}{d\nu} = \Phi_2\gamma' + \Phi_1\omega' + \Phi_4 = 0$, where $\Phi_1 = 3\gamma^2 - 3\omega^2 + 2V_1\gamma + V_2$, $\Phi_2 = 6\gamma\omega + 2V_1\omega$, $\Phi_3 = (\gamma^2 - \omega^2)V_1' + \gamma V_2' + V_3'$, $\Phi_4 = 2\gamma\omega V_1' + \omega V_2'$. From the second equation of (4.12) we note that at ν^*, $3\gamma^2 - \omega^2 + 2V_1\gamma + V_2 = 0$, hence $\Phi_1(\nu^*) = 0$. With $\Phi_1 = 0$, solving for γ' and ω' gives $\gamma'(\nu^*) = \frac{\Phi_4}{\Phi_2}$, $\omega'(\nu^*) = -\frac{\Phi_3}{\Phi_2}$. Substituting these into (4.11) yields $\gamma\omega' - \omega\gamma' = \gamma\left(-\frac{\Phi_3}{\Phi_2}\right) - \omega\left(\frac{\Phi_4}{\Phi_2}\right) = -\frac{\gamma\Phi_3 + \omega\Phi_4}{\Phi_2}$. Thus the transversality condition (4.11) becomes

$$\gamma(\nu^*)\Phi_3(\nu^*) + \omega(\nu^*)\Phi_4(\nu^*) \neq 0. \tag{4.13}$$

Therefore, the system (3.1) undergoes a Hopf bifurcation at the equilibrium Ω^* as the parameter ν crosses the critical value ν^*. The numerical results in Section 5 confirm that the bifurcation is supercritical, leading to the emergence of stable limit cycles. Figures 3, 6, 9, 12, and 15 demonstrate that as ν passes through ν^*, the complex eigenvalues cross the stability boundary $|\arg(\phi)| = \eta\pi/2$. □

4.3. **Global stability of the system.**

Theorem 4.6. *The coexistence equilibrium point $\Omega(P_x, P_y, P_z) = (P_x^*, P_y^*, P_z^*)$ is globally asymptotically stable.*

Proof. Let us define a function,

$$\chi(P_x, P_y, P_z) = \left(P_x - P_x^* - P_x^* \ln\frac{P_x}{P_x^*}\right) + \beta_1\left(P_y - P_y^* - P_y^* \ln\frac{P_y}{P_y^*}\right) + \beta_2\left(P_z - P_z^* - P_z^* \ln\frac{P_z}{P_z^*}\right),$$

where, a continuous function $\chi > 0$ for all values of $(P_x, P_y, P_z) \neq (P_x^*, P_y^*, P_z^*)$ and $\chi = 0$ only at (P_x^*, P_y^*, P_z^*) and $\beta_1 > 0, \beta_2 > 0$ implies that

$$\begin{aligned}
D_t^\eta\chi(P_x, P_y, P_z) &= \left(\frac{P_x - P_x^*}{P_x}\right) D_t^\eta P_x(t) + \beta_1\left(\frac{P_y - P_y^*}{P_y}\right) D_t^\eta P_y(t) + \beta_2\left(\frac{P_z - P_z^*}{P_z}\right) D_t^\eta P_z(t)\\
&\leq \left(\frac{P_x - P_x^*}{P_x}\right)\frac{rP_x}{1+g_1P_x}\left(1 - \frac{P_x}{k}\right) - \frac{(1+g_2P_y)(1+w_f)P_xP_y}{1+h(1+g_2P_y)(1+w_f)P_x}\\
&+ \beta_1\left(\frac{P_y - P_y^*}{P_y}\right)\frac{(1+g_2P_y)(1+w_f)P_xP_y}{1+h(1+g_2P_y)(1+w_f)P_x} - \frac{\delta P_yP_z}{P_y+P_z} - m_1P_y\\
&+ \beta_2\left(\frac{P_z - P_z^*}{P_z}\right)\frac{\delta P_yP_z}{P_y+P_z} - m_2P_z\\
&\leq (P_x - P_x^*)\left(\frac{r}{1+g_1P_x}\left(1 - \frac{P_x}{k}\right) - \frac{(1+g_2P_y)(1+w_f)P_y}{1+h(1+g_2P_y)(1+w_f)P_x}\right.\\
&\left. - \frac{r}{1+g_1P_x^*}\left(1 - \frac{P_x^*}{k}\right) + \frac{(1+g_2P_y^*)(1+w_f)P_y^*}{1+h(1+g_2P_y^*)(1+w_f)P_x^*}\right)\\
&+ \beta_1(P_y - P_y^*)\left(\frac{(1+g_2P_y)(1+w_f)P_x}{1+h(1+g_2P_y)(1+w_f)P_x} - \frac{\delta P_z}{P_y+P_z}\right.\\
&\left. - \frac{(1+g_2P_y^*)(1+w_f)P_x^*}{1+h(1+g_2P_y^*)(1+w_f)P_x^*} + \frac{\delta P_z^*}{P_y^*+P_z^*}\right)\\
&+ \beta_2(P_z - P_z^*)\left(\frac{\delta P_y}{P_y+P_z} - \frac{\delta P_y^*}{P_y^*+P_z^*}\right)\\
&\leq (P_x - P_x^*)\left[\frac{-r(g_1k+1)(P_x - P_x^*)}{k(1+g_1P_x)(1+g_1P_x^*)} - \frac{(1+w_f)(P_y - P_y^*)}{r_1r_2}\right.\\
&- \frac{g_2(1+w_f)(P_y + P_y^*)(P_y - P_y^*)}{r_1r_2} - \frac{h(1+g_2P_y)(1+g_2P_y^*)(1+w_f)^2P_x(P_y - P_y)^*}{r_1r_2}\\
&\left. - \frac{[h(1+g_2P_y)(1+g_2P_y^*)(1+w_f)^2P_y(P_x - P_x^*)]}{r_1r_2}\right]
\end{aligned}$$

$$
\begin{aligned}
&+ \left(P_y - P_y^*\right)\left[\frac{(1+g_2P_y)(1+w_f)(P_x-P_x^*)}{r_1r_2} + \frac{g_2(1+w_f)P_x^*(P_y-P_y^*)}{r_1r_2}\right.\\
&\left.+ \frac{\beta_1\delta P_z(P_y-P_y^*)}{(P_y+P_z)(P_y^*+P_z^*)} - \frac{\beta_1\delta P_y(P_z-P_z^*)}{(P_y+P_z)(P_y^*+P_z^*)} - \beta_1 m_1\right]\\
&+ (P_z - P_z^*)\left[-\frac{\beta_2\delta P_y(P_z-P_z^*)}{(P_y+P_z)(P_y^*+P_z^*)} + \frac{\beta_2\delta P_z(P_y-P_y^*)}{(P_y+P_z)(P_y^*+P_z^*)} - \beta_2 m_2\right]\\
&\le -\left[\frac{r(g_1k+1)(P_x-P_x^*)}{k(1+g_1P_x)(1+g_1P_x^*)} + \frac{\left[h(1+g_2P_y)(1+g_2P_y^*)(1+w_f)^2P_y(P_x-P_x^*)\right]}{r_1r_2}\right](P_x-P_x^*)^2\\
&+ \left[\frac{\beta_1g_2(1+w_f)P_x^*}{r_1r_2} + \frac{\beta_1\delta P_z}{(P_y+P_z)(P_y^*+P_z^*)}\right](P_y-P_y^*)^2\\
&- \left[\frac{(1+w_f)}{r_1r_2} + \frac{\left[h(1+g_2P_y)(1+g_2P_y^*)(1+w_f)^2P_y\right]}{r_1r_2}\right](P_x-P_x^*)(P_y-P_y^*)\\
&- \left[\frac{\delta\beta_2P_z - \delta\beta_1P_y}{(P_y+P_z)(P_y^*+P_z^*)}\right](P_y-P_y^*)(P_z-P_z^*)\\
&- m_1(P_y-P_y^*) - m_2(P_z-P_z^*)\\
&\le -\left[\frac{r(g_1k+1)(P_x-P_x^*)}{k(1+g_1P_x)(1+g_1P_x^*)} + \frac{\left[h(1+g_2P_y)(1+g_2P_y^*)(1+w_f)^2P_y(P_x-P_x^*)\right]}{r_1r_2}\right.\\
&\left.+ \frac{1}{2}\frac{(1+w_f)}{r_1r_2} + \frac{\left[h(1+g_2P_y)(1+g_2P_y^*)(1+w_f)^2P_y\right]}{r_1r_2}\right](P_x-P_x^*)^2\\
&- \left[\frac{1}{2}\frac{(1+w_f)}{r_1r_2} + \frac{\left[h(1+g_2P_y)(1+g_2P_y^*)(1+w_f)^2P_y\right]}{r_1r_2} + \frac{1}{2}\frac{\delta\beta_2P_z-\delta\beta_1P_y}{(P_y+P_z)(P_y^*+P_z^*)}\right.\\
&\left.+ \frac{\beta_1g_2(1+w_f)P_x^*}{r_1r_2}\right](P_y-P_y)^2 - \left[\frac{\beta_1g_2(1+w_f)P_x^*}{r_1r_2}\right](P_z-P_z^*)^2.
\end{aligned}
$$

Since the feasible region $\Phi \subset \mathbb{R}^3_+$ is compact. By Theorem 3.2 it is positively invariant with respect to system (3.1), and the Lyapunov function $\chi(P_x, P_y, P_z)$ is continuously differentiable on Φ, we have established that ${}^cD_t^\eta\chi(P_x, P_y, P_z) \le 0 \quad \forall (P_x, P_y, P_z) \in \Phi$, with equality holding if and only if $(P_x, P_y, P_z) = (P_x^*, P_y^*, P_z^*) = \mathcal{E}^*$. Define the set $\mathcal{S} = \{(P_x, P_y, P_z) \in \Phi : {}^cD_t^\eta\chi(P_x, P_y, P_z) = 0\} = \{\mathcal{E}^*\}$. Since $\mathcal{E}^*$ is itself an equilibrium point, it is invariant. Hence, the largest invariant set contained in $\mathcal{S}$ is $\mathcal{M} = \{\mathcal{E}^*\}$. By the fractional LaSalle invariance principle [16], every solution of system (3.1) initiating in Φ converges to $\mathcal{M}$ as $t \to \infty$. That is: $\lim_{t\to\infty}\left(P_x(t), P_y(t), P_z(t)\right) = (P_x^*, P_y^*, P_z^*)$. It is concluded that the coexistence equilibrium $\mathcal{E}^* = (P_x^*, P_y^*, P_z^*)$ is globally asymptotically stable in the feasible region Φ. Therefore The coexistence equilibrium $\mathcal{E}^*$ is globally asymptotically stable in Φ. □

5. Numerical simulations

Numerical simulations allow researchers to investigate the system's behavior under different situations when analytical solutions are impractical due to the inherent nonlinearities provided by fractional-order derivatives. In this section, a numerical method is approached to evaluate the theoretical results of our fractional-order model, which includes disease-mediated predator-prey interactions under climatic stressors. The simulations are carried out in MATLAB, using the Fractional Linear Multi-Step Method (FLMM) via the FLMM2 toolbox; specifically, a predictor-corrector scheme is used to estimate the accurate, stable solutions to the Caputo fractional differential equations [5, 6]. Parameter values were chosen for numerical illustration within biologically plausible ranges, consistent with prior fractional ecological models [2, 9, 17, 26, 27]. These simulations reveal nonlinear phenomena such as supercritical Hopf bifurcations, where minimal parameter changes result in substantial dynamical shifts, in addition to validating our analytical stability criteria.

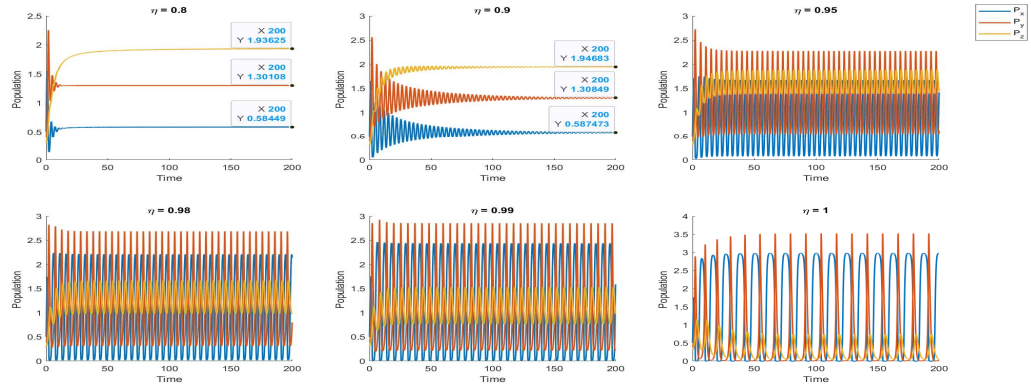

FIGURE 1. The solutions showing the time series plot for the numerical simulations of the system (3.1) for varying the $\eta = [0.8, 0.9, 0.95, 0.98, 0.99, 1]$.

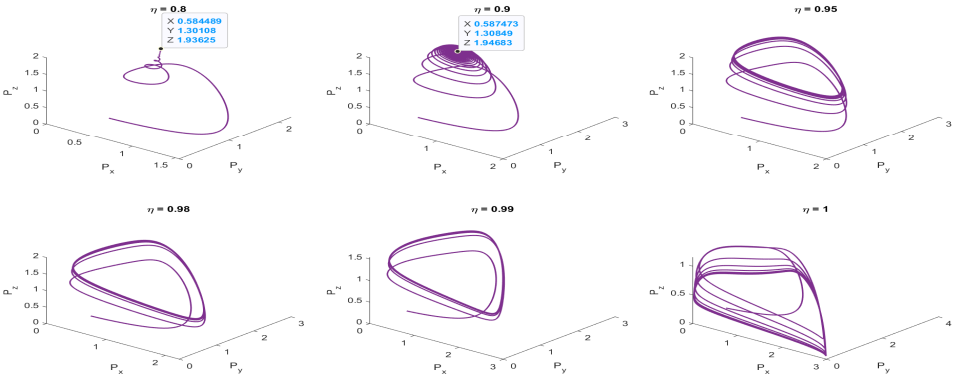

FIGURE 2. The solutions showing the phase portrait plot for the numerical simulations of the system (3.1) for varying the $\eta = [0.8, 0.9, 0.95, 0.98, 0.99, 1]$.

5.1. **Impact of fractional order η.** Here, we conduct numerical simulations to validate the impact of the fractional order by varying its parameter value η. Choosing it as a bifurcation parameter, we observe its influence on the system's stability. The parameter values used are: $r = 5$, $k = 3$, $g_1 = 0.5$, $g_2 = 0.5$, $w_f = 1.5$, $h = 0.3$, $\delta = 1.5$, $m_1 = 0.5$, $m_2 = 0.6$, with a step size of $h = 2^{-6}$. The fractional order parameter is varied as $\eta = [0.8, 0.9, 0.95, 0.98, 0.99, 1]$, with initial conditions $(P_{x_0}, P_{y_0}, P_{z_0}) = (0.5, 0.4, 0.3)$, the stability behavior is then analyzed. Figure 1 shows a time series plot, illustrating that as the fractional parameter η increases, the system transitions gradually from a stable to an unstable state. This transition occurs due to a Hopf bifurcation, where increasing values of a parameter η destabilize the previously stable equilibrium. Figure 2 presents the corresponding phase portraits, confirming that the bifurcation direction is supercritical (forward). Consequently, increasing η induces a shift from stability to instability, potentially reducing predation efficiency and causing a decline in population density. This demonstrates that the system (3.1) is locally asymptotically stable for lower values of η. In Figure 3, by Theorem 4.5, varying the parameter value with respect to η, the hopf bifurcation point occurs at the equilibrium point, $[0.584, 1.301, 1.946]$ showing a supercritical Hopf bifurcation shifting from stability to instability.

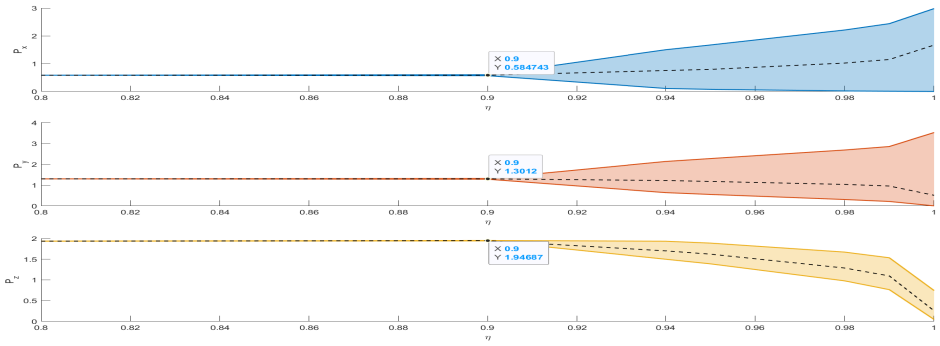

FIGURE 3. Bifurcation diagram of the system (3.1) with respect to η.

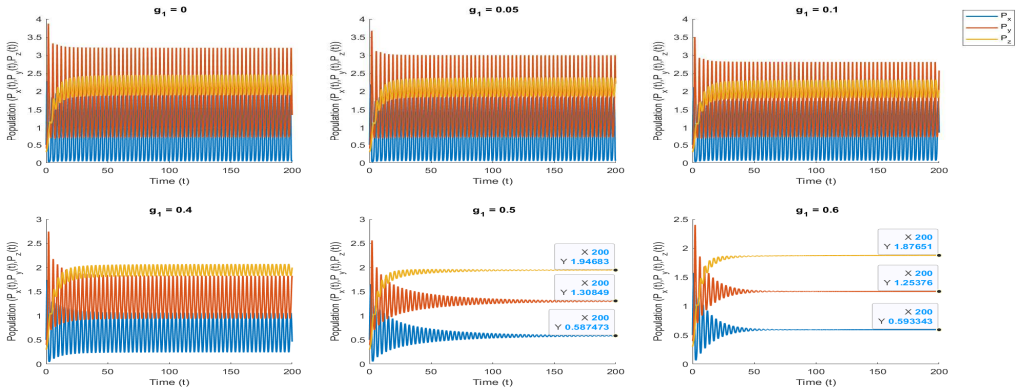

FIGURE 4. The solutions showing the time series plot for the numerical simulations of the system (3.1) for varying the $g_1 = [0, 0.05, 0.1, 0.4, 0.5, 0.6]$.

5.2. **Impact of global warming g_1 on prey density P_x.** We conduct numerical simulations to validate the impact of global warming g_1 on prey density by P_x varying its parameter value. Choosing it as a bifurcation parameter, we observe its influence on the system's stability. The parameter values used are: $\eta = 0.9$, $r = 5$, $k = 3$, $g_2 = 0.5$, $w_f = 1.5$, $h = 0.3$, $\delta = 1.5$, $m_1 = 0.5$, $m_2 = 0.6$, with a step size of $h = 2^{-6}$. The global warming parameter P_x is varied as $g_1 = [0, 0.05, 0.1, 0.4, 0.5, 0.6]$, with initial conditions $(P_{x_0}, P_{y_0}, P_{z_0}) = (0.5, 0.4, 0.3)$, the stability behavior is then analyzed. Figure 4 reveals distinct behavioral regimes: for $g_1 \in [0, 0.4]$, the population densities $P_x(t)$, $P_y(t)$, and $P_z(t)$ exhibit a stable limit cycle because of persistent oscillatory dynamics. As g_1 approaches 0.5, the intensity of limit cycle oscillations decreases, leading the bifurcation to occur. When it g_1 reaches 0.6, the convergence of all trajectories to constant equilibrium values signifies the onset of a stable steady state. In Figure 5, for $g_1 < 0.5$, the trajectories form closed periodic orbits, showing a limit cycle. Beyond the critical threshold $g_1 \geq 0.6$, these orbits decreases to a stable point, reflecting the system's stabilization. This change in dynamics qualitatively resembles a supercritical Hopf bifurcation, in which the system undergoes a smooth transition from cyclic behavior to a steady state as g_1 increases. Higher values of g_1 lead to damping of the oscillatory behavior, with the system evolving toward an asymptotically stable state. This parameter-dependent bifurcation suggests that prey populations may transition from small-amplitude periodic oscillations to steady-state equilibria in response to environmental or biological constraints. In Figure 6, by Theorem 4.5, varying the parameter value with respect to g_1, the Hopf bifurcation point occurs at the equilibrium point $[0.584, 1.301, 1.946]$ showing a supercritical Hopf bifurcation shifting from instability to stability.

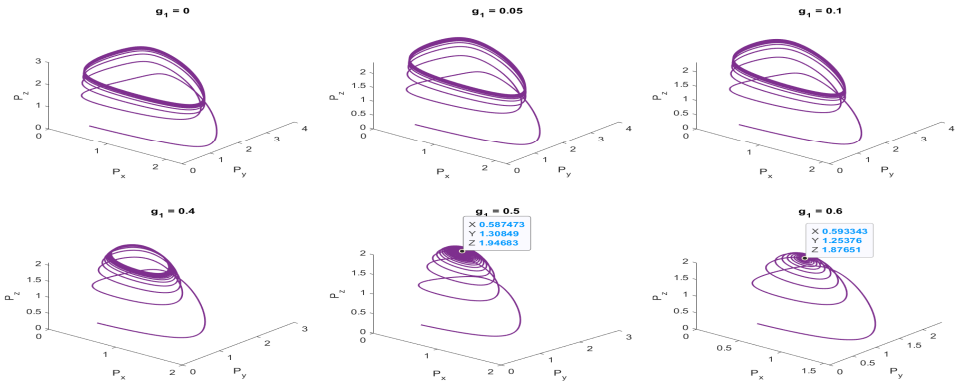

FIGURE 5. The solutions showing the phase portrait plot for the numerical simulations of the system (3.1) for varying the $g_1 = [0, 0.05, 0.1, 0.4, 0.5, 0.6]$.

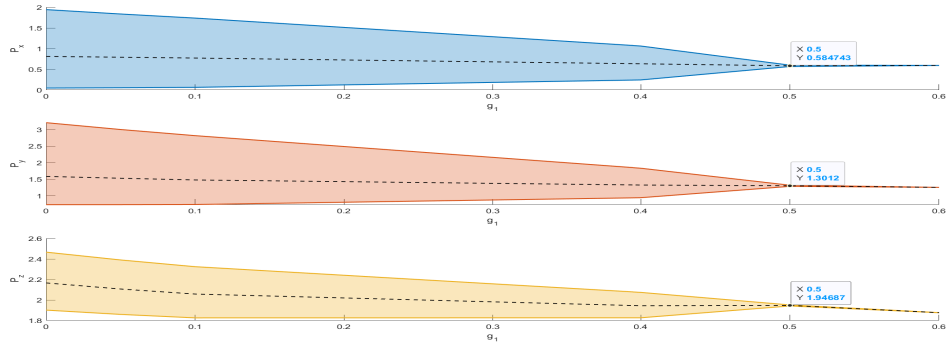

FIGURE 6. Bifurcation diagram ofthe system (3.1) with respect to g_1.

5.3. **Impact of global warming g_2 on the meso predator density P_y.** We conduct numerical simulations to validate the impact of the global warming parameter g_2 on the meso predator density P_y by varying its parameter value. Choosing g_2 as a bifurcation parameter, we observe its influence on the system's stability. The parameter values used are: $\eta = 0.9$, $r = 5$, $k = 3$, $g_1 = 0.5$, $w_f = 1.5$, $h = 0.3$, $\delta = 1.5$, $m_1 = 0.5$, $m_2 = 0.6$, with a step size of $h = 2^{-6}$. The global warming parameter on P_y is varied as $g_2 = [0.3, 0.5, 0.7, 0.9, 1, 2]$. With initial conditions $(P_{x_0}, P_{y_0}, P_{z_0}) = (0.5, 0.4, 0.3)$, the system's stability behavior is analysed. In Figure 7, for $0.3 \leq g_2 \leq 0.5$, the system exhibits damped oscillatory behavior and approaches an asymptotically stable equilibrium state. However, for $g_2 \geq 0.7$, above a critical value, the trajectories become persistent limit cycles, with the size of oscillations being a monotonically increasing function of g_2. This qualitative change, along with the appearance of non-decaying periodic solutions, confirms the presence of a supercritical Hopf bifurcation. In Figure 8, at lower values of g_2, the phase portraits exhibit inward spiraling trajectories, indicating damped oscillations where the system gradually settles into a stable fixed point. However, as g_2 approaches and exceeds approximately 0.7, the trajectories evolve into closed loops, marking the emergence of sustained periodic oscillations. This transition suggests the onset of a supercritical Hopf bifurcation, where the system loses stability at the fixed point and gives rise to a stable limit cycle. Beyond this threshold, particularly for $g_2 = 0.9, 1$, and 2, the closed trajectories become well-defined and persistent, confirming that the system has entered a regime of undamped, self-sustained oscillations. Thus, the figure clearly demonstrates how varying g_2 governs the shift from equilibrium dynamics to continuous oscillatory behavior. In Figure 9, by

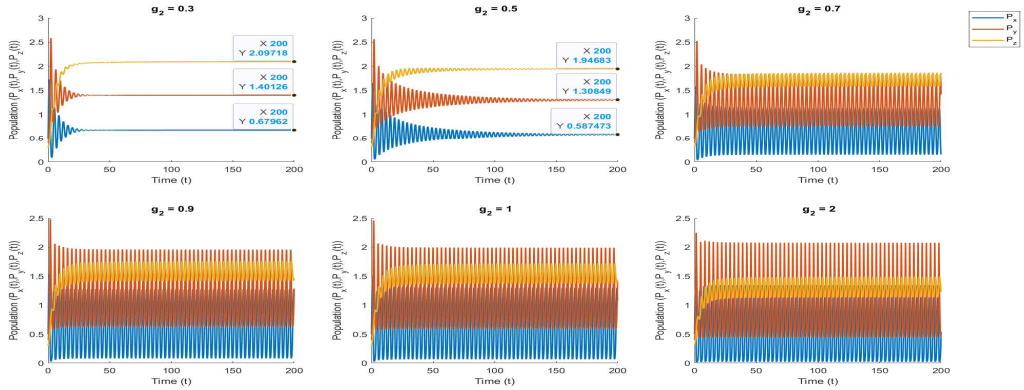

FIGURE 7. The solutions showing the time series plot for the numerical simulations of our system (3.1) for varying the $g_2 = [0.3, 0.5, 0.7, 0.9, 1, 2]$.

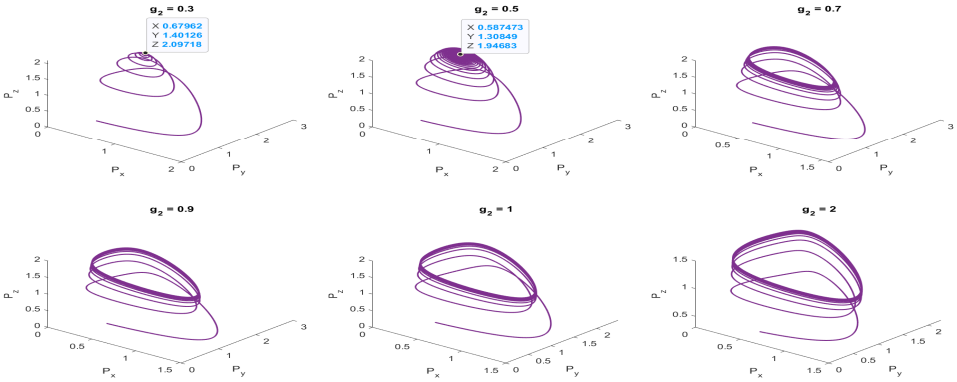

FIGURE 8. The solutions showing the phase portrait plot for the numerical simulations of the system (3.1) for varying the $g_2 = [0.3, 0.5, 0.7, 0.9, 1, 2]$.

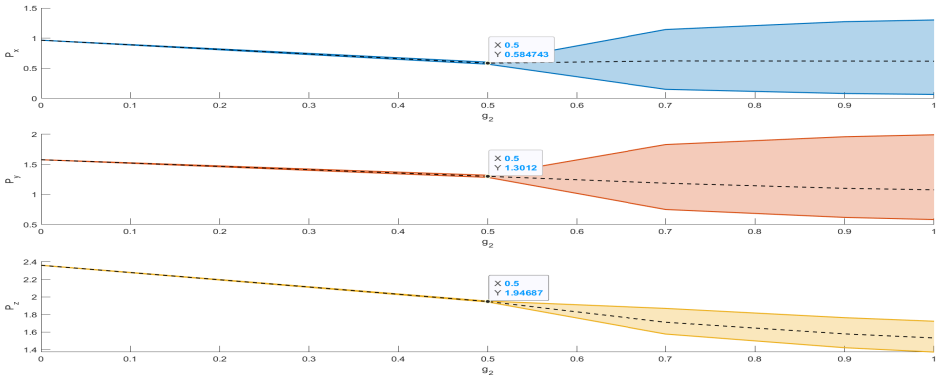

FIGURE 9. Bifurcation diagram of the system (3.1) with respect to g_2.

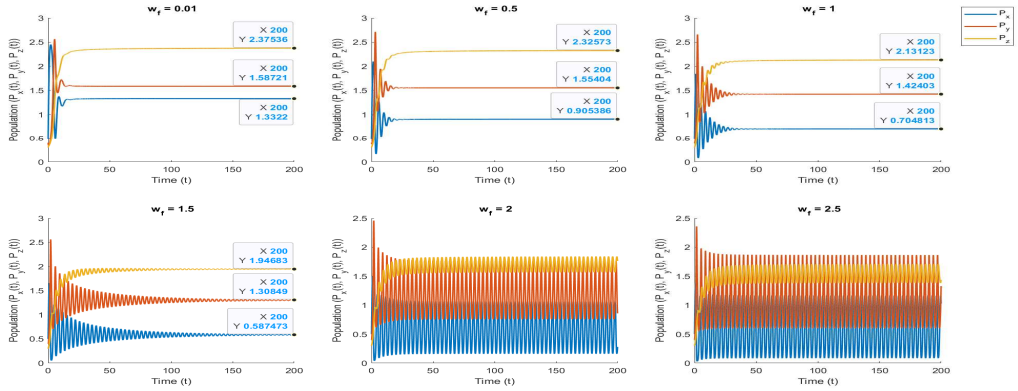

FIGURE 10. The solutions showing the time series plot for the numerical simulations of the system (3.1) for varying the $w_f = [0.01, 0.5, 1.0, 1.5, 2.0, 2.5]$.

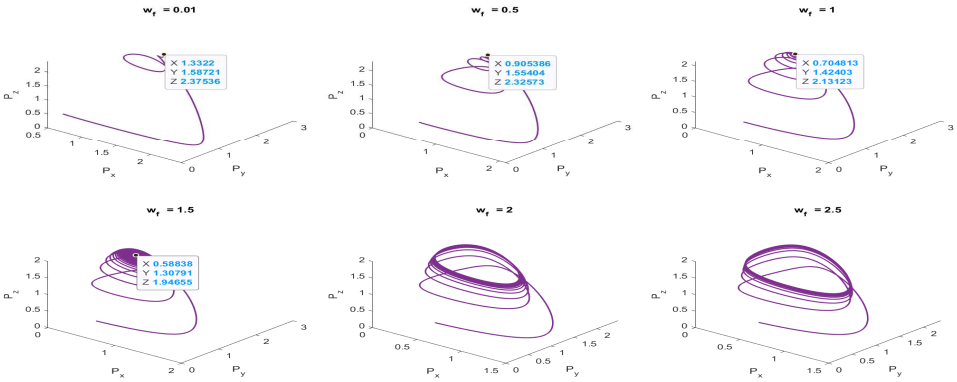

FIGURE 11. The solutions showing the phase portrait plot for the numerical simulations of the system (3.1) for varying the $w_f = [0.01, 0.5, 1.0, 1.5, 2.0, 2.5]$.

Theorem 4.5, varying the parameter value with respect to g_2, the hopf bifurcation point occurs at the equilibrium point $[0.584, 1.301, 1.946]$ showing a supercritical Hopf bifurcation shifting from instability to stability.

5.4. **Impact of wind flow w_f on the meso predator density P_y.** We conduct numerical simulations to validate the impact of the wind flow w_f on the meso predator density P_y varying its parameter value. Choosing it as a bifurcation parameter, we observe its influence on the system's stability. The parameter values used are: $\eta = 0.9$, $r = 5$, $k = 3$, $g_1 = 0.5$, $g_2 = 0.5$, $h = 0.3$, $\delta = 1.5$, $m_1 = 0.5$, $m_2 = 0.6$, with a step size of $h = 2^{-6}$. The windflow parameter is varied as $w_f = [0.01, 0.5, 1.0, 1.5, 2.0, 2.5]$, with initial conditions $(P_{x_0}, P_{y_0}, P_{z_0}) = (0.5, 0.4, 0.3)$, the stability behavior is then analysed. In Figure 10, for smaller values of w_f from 0.01 to 1, the system shows damped oscillations, which progressively converge to a asymptotic steady-state equilibrium. We see a qualitative change as w_f rises to 1.5, the oscillations keep happening with a constant amplitude instead of decaying, indicating the onset of limit cycle behavior. In the dynamics of the system, this represents a bifurcation point. The system settles into persistent, regular periodic oscillations for even higher values $w_f = 2$ and $w_f = 2.5$, indicating the existence of a stable periodic orbit. Wind flow introduces a cyclic control in predator-prey interactions, as seen by the more prominent oscillation amplitudes in each population variable. In Figure 11, the damped behavior is consistent with trajectories

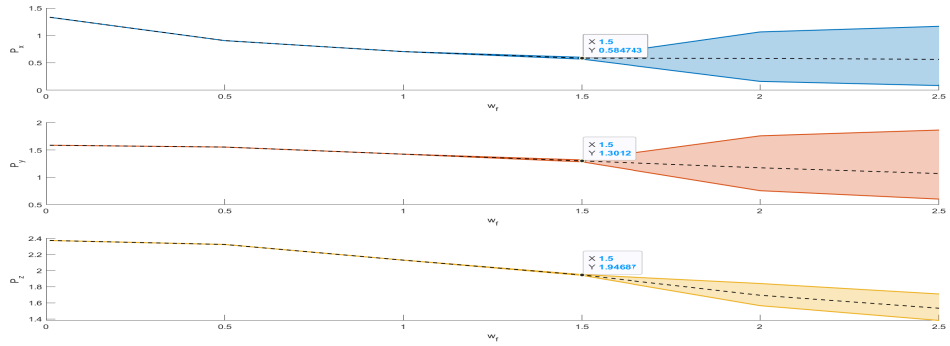

FIGURE 12. Bifurcation diagram of the system (3.1) with respect to w_f.

for lower w_f values spiralling inward toward a fixed point. When w_f rises to 1.5, a supercritical Hopf bifurcation starts as the trajectories start to form closed cycles. The system exhibits persistent closed cycles at $w_f = 2$ and $w_f = 2.5$, which is beyond this threshold and validates the stable limit cycles. The larger and more stable these trajectories get as w_f rises, suggesting that the oscillatory behavior gets more intense and organised as wind flow increases. In Figure 12, by Lemma Theorem (4.5), varying the parameter value with respect to w_f, the hopf bifurcation point occurs at the equilibrium point $[0.584, 1.301, 1.946]$ showing a supercritical Hopf bifurcation shifting from instability to stability.

5.5. **Impact of disease transmission rate δ on apex predator density P_z.** We conduct numerical simulations to validate the impact of the disease transmission rate δ on the apex predator density P_z varying its parameter value. Choosing it as a bifurcation parameter, we observe its influence on the system's stability. The parameter values used are: $\eta = 0.9$, $r = 5$, $k = 3$, $g_1 = 0.5$, $g_2 = 0.5$, $h = 0.3$, $w_f = 1.5$, $m_1 = 0.5$, $m_2 = 0.6$, with a step size of $h = 2^{-6}$. The rate of disease transmission parameter is varied as $\delta = [0, 0.5, 0.9, 0.95, 0.99, 1]$, with initial conditions $(P_{x_0}, P_{y_0}, P_{z_0}) = (0.5, 0.4, 0.3)$, the stability behavior is then analyzed. In Figure 13, at lower values of δ (e.g., $\delta = 0$ and $\delta = 0.5$), where transient oscillations decay rapidly and the populations converge monotonically to steady-state values, the dynamics are characterized by strong damping. There is minimal population transfer into that state, as indicated by the P_z component as very small in this regime. However, when δ approaches unity ($\delta = 0.9$ to $\delta = 1$), the system destabilizes, all three population variables exhibit persistent, periodic oscillations in place of the damped oscillations. This sustained rhythmic behavior signals the onset of a limit cycle, a key indicator of a Hopf bifurcation. As δ increases, the amplitude of these oscillations increases, but the periodicity endures consistent, demonstrating that the system persists in a limit cycle regime, and the populations stabilize at new steady-state values. Population accumulation and significant asymptotic stability result from longer periods of persistent oscillations. In Figure 14, for low values $\delta = 0$ to 0.5, the trajectories quickly converge to a fixed point near the $P_z = 0$ plane, reflecting strong damping and negligible population in P_z. As δ increases from 0.9 to 1, the spirals widen and persist longer, stabilizing at higher P_z values. At near-resonant conditions $\delta = 0.99$ to 1, the system transitions to sustained quasi-limit cycles, exhibiting underdamped oscillations and intricate population exchange. This evolution demonstrates a clear transition from a heavily damped regime to a dynamic oscillatory phase, with increasing participation of the P_z state as δ approaches unity. This indicates a fundamental change in the dynamical regime of the system and visually validates a Hopf bifurcation-like transition from a fixed point equilibrium to a limit cycle as increases. As δ increases , the phase space trajectory decreases and resolves into a different steady point, showing that the periodic orbit has vanished and a new stable equilibrium has been established. These qualitative across δ values provide strong evidence of a Hopf bifurcation occurring around $\delta = 1$, where a fixed point loses stability and gives rise to a limit cycle. In Figure 15, by Theorem 4.5, varying the parameter value with respect to δ, the Hopf bifurcation point occurs at the equilibrium point $[0.584, 1.301, 1.946]$ showing a supercritical Hopf bifurcation shifting from instability to stability.

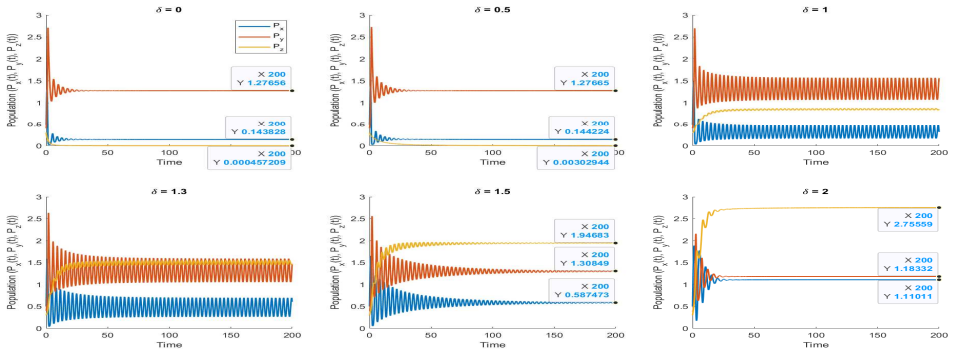

FIGURE 13. The solutions showing the time series plot for the numerical simulations of the system (3.1) for varying the $\delta = [0, 0.5, 0.9, 0.95, 0.99, 1]$.

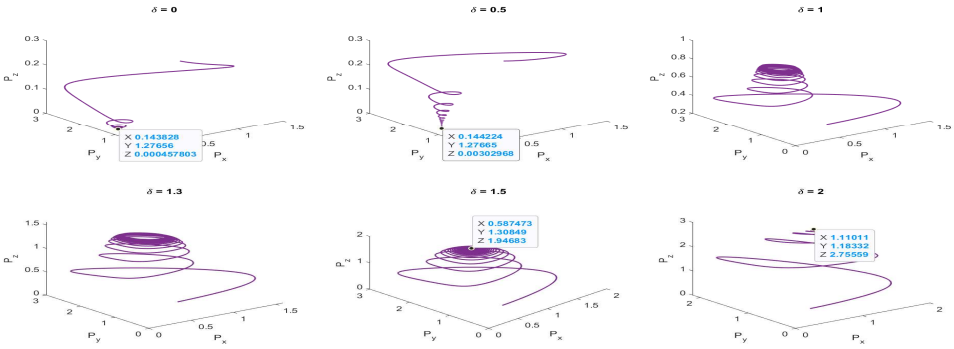

FIGURE 14. The solutions showing the phase portrait plot for the numerical simulations of the system (3.1) for varying the $\delta = [0, 0.5, 0.9, 0.95, 0.99, 1]$.

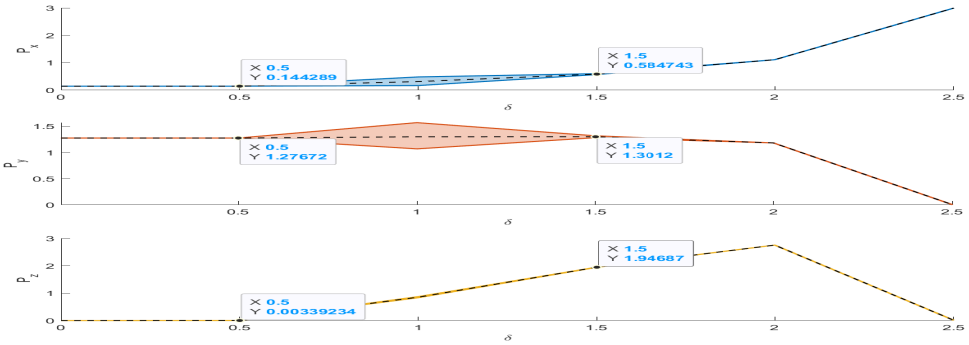

FIGURE 15. Bifurcation diagram of the system (3.1) with respect to δ.

6. Conclusion

In this framework, fractional-order dynamical system modeling disease-mediated predator-prey interactions under climatic stressors is proposed. The qualitative behavior of the system is investigated by proving the existence of a unique well-defined solution and non-negative confined solutions. Then, the biologically feasible equilibrium points and the computed Jacobian matrix helps in examining the local and global stability analysis. Later, in the next section, we conducted comprehensive numerical simulations to validate our theoretical findings, demonstrating that the analytical results remain robust under varying parametric influences. Critical dynamical transitions controlled by key parameters are revealed by the numerical simulations: changes in the fractional order η cause Hopf bifurcations, which move the system from stability to sustained oscillations, while increasing global warming g_1, g_2 and wind flow w_f destabilize equilibria, causing limit cycles or damping effects. Higher rates of disease transmission δ destabilize predator populations while stabilizing prey through less predation pressure, exhibiting a threshold-driven bifurcation. When taken together, these findings show that climatic stresses, epidemiological interactions, and memory effects via $\eta, g_1, g_2, w_f, \delta$ all nonlinearly alter ecosystem resilience. To further establish this concept as a foundation for ecological forecasting of the next generation, further additions can include stochastic climatic forcing or spatiotemporal heterogeneities.

Authors contribution

M. Sivaranjani: Writing—original draft; methodology; investigation; validation; conceptualization; software; visualization.

M. Sambath: Supervision; validation; formal analysis; conceptualization; investigation; visualization.

K. Balachandran: critical analysis and reviewing the text.

Funding Information

The work of first author is supported by the University Research Fellowship (URF), Periyar University, Salem and she is thankful to the University for providing the financial support.

Conflict of Interest

The authors declare that they have no conflict of interest.

References

[1] K. Balachandran, *An Introduction to Fractional Differential Equations*, Springer, Singapore, (2023).
[2] D. Barman, J. Roy, and S. Alam, *Impact of wind in the dynamics of prey–predator interactions*, Mathematics and Computers in Simulation, *191* (2022), 49-81.
[3] S.K. Choi, B. Kang, and N. Koo, *Stability for Caputo fractional differential systems*, Abstract and Applied Analysis, *2014*(1) (2014), 631419.
[4] X. Gao, Q. Pan, M. He, and Y. Kang, *A predator–prey model with diseases in both prey and predator*, Physica A: Statistical Mechanics and its Applications, *392*(23) (2013), 5898-5906.
[5] R. Garrappa, *Numerical solution of fractional differential equations: A survey and a software tutorial*, Mathematics, *6*(2) (2018), 16.
[6] R. Garrappa, *FLMM2*, MATLAB Central File Exchange, (2021).
[7] M. Haque, *A predator–prey model with disease in the predator species only*, Nonlinear Analysis: Real World Applications, *11*(4) (2010), 2224-2236.
[8] Z. Hammouch, M. O. Jamil, and C. Unlu, *Dynamics investigation and numerical simulation of fractional-order predator-prey model with Holling type II functional response*, Discrete and Continuous Dynamical Systems-S, *18*(5) (2025), 1230-1266.
[9] C. S. Holling, *The functional response of predator to prey density and its role in mimicry and population regulation*, Memoirs of the Entomological Society of Canada, *97*(S45) (1965), 5–60.

[10] Y. H. Hsieh and C. K. Hsiao, *Predator–prey model with disease infection in both populations*, Mathematical Medicine and Biology: a Journal of the IMA, *25*(3) (2008), 247-266.
[11] S. Jana and T. K. Kar, *Modeling and analysis of a prey–predator system with disease in the prey*, Chaos, Solitons and Fractals, *47* (2013), 42-53.
[12] B. B. Kamaland A. Mustafa, *Dynamical Analysis of a Three Species Food-WebModel With Extended Holling Type II Functional Response*, European Journal of Pure and Applied Mathematics, *18*(1) (2025), 5397-5397.
[13] S. Karthikeyan, P. Ramesh, and M. Sambath, *Stability analysis of fractional-order predator-prey model with anti-predator behaviour and prey refuge*, Journal of Mathematical Modeling (JMM), *11*(3) (2023), 527-546.
[14] A. Kilbas, H. Srivastava and J. Trujillo, *Theory and Applications of Fractional Differential Equations*, Elsevier, New York, (2006).
[15] R. Khoshsiar Ghaziani and J. Alidousti, *Stability analysis of a fractional order prey-predator system with non-monotonic functional response*, Computational Methods for Differential Equations,*4*(2) (2016), 151-161.
[16] J. La Salle and S. Lefschetz, *Stability by Liapunov's direct method with applications by Joseph L Salle and Solomon Lefschetz*, Elsevier, *4* (2012).
[17] A. N. Laws, *Climate change effects on predator–prey interactions*, Current opinion in insect science, *23*(1) (2017), 28-34.
[18] P. Panja, *Can global warming change predator-prey dynamics: A modelling study*, International Journal of Big Data Mining for Global Warming, *5*(1) (2023), 2350001.
[19] P. Panja, *Impacts of wind and anti-predator behaviour on predator-prey dynamics: a modelling study*, International Journal of Computing Science and Mathematics, *15*(4) (2022), 396-407.
[20] I. Petras, *Fractional-Order Nonlinear Systems: Modeling, Analysis and Simulation*, Higher Education Press, Beijing, (2011).
[21] I. Podlubny, *Fractional Differential Equations*, Academic Press, London, (1999).
[22] E. Post, R. O. Peterson, and N. C. Stenseth, B. E. McLaren, *Ecosystem consequences of wolf behavioural response to climate*, Nature, *401*(6756) (1999), 905–907.
[23] B. C. Rall, O. Vucic-Pestic, R. B. Ehnes, M. Emmerson, and U. Brose, *Temperature, predator–prey interaction strength and population stability*, Global Change Biology, *16*(8) (2010), 2145-2157.
[24] P. Ramesh, M. Sambath, M. H. Mohd and K. Balachandran, *Stability analysis of the fractional order prey-predator model with infection*, International Journal of Modelling and Simulation, *4*1(6) (2021), 434-450.
[25] P. Ramesh, M. Sambath and K. Balachandran, *Hopf bifurcation and synchronization of a fractional order butterfly-fish chaotic system*, Journal of Control and Decision, *9*(1) (2022), 117-128.
[26] F. A. Rihan, S. Lakshmanan, A. H. Hashish, R. Rakkiyappan, and E. Ahmed, *Fractional-order delayed predator–prey systems with Holling type-II functional response*, Nonlinear Dynamics, *80* (2015), 777-789.
[27] Y. Sekerci, *Climate change effects on fractional order prey-predator model*, Chaos, Solitons and Fractals, *134* (2020), 109690.
[28] M. Sivaranjani and M. Sambath, *Asymptotic Behavior of Fractional-Order Holling Type II Prey-Predator With Hunting Cooperation*, Mathematical Methods in the Applied Sciences, *48*(14) (2025), 13718-13732.
[29] A. H. Surosh, R. Khoshsiar Ghaziani, and J. Alidoosti, *Dynamics and bifurcation control of a fractional-order delayed predator–prey model with an omnivore*, Computational Methods for Differential Equations, (2024).
[30] A. A. Thirthar, S. Jawad, S. J. Majeed, and K. S. Nisar, *Impact of wind flow and global warming in the dynamics of prey–predator model*, Results in Control and Optimization, *15* (2024), 100424.
[31] A. A. Thirthar, N. Sk, B. Mondal, and M. A. Alqudah, *Utilizing memory effects to enhance resilience in disease-driven prey-predator systems under the influence of global warming*, Journal of Applied Mathematics and Computing, *69*(6) (2023), 4617-4643.
[32] G. R. Walther, E. Post, P. Convey, A. Menzel, C. Parmesan, and T. J. Beebee, *Ecological responses to recent climate change*, Nature, *416*(6879) (2002), 389-395.
[33] M. Zimova, L. S. Mills, and J. J. Nowak, *High fitness costs of climate change-induced camouflage mismatch*, Ecology letters, *19*(3) (2016), 299-307.